FULL PAPER

Highly Robust Lithium Ion Battery Anodes from Lignin: An Abundant, Renewable, and Low-Cost Material

Wyatt E. Tenhaeff, Orlando Rios, Karren More, and Michael A. McGuire*

The synthesis, processing, and performance of a low-cost monolithic battery electrode, produced entirely of natural and renewable resources, are reported. This anode material exhibits tunable electrochemical performance suitable for both high power and high energy applications. A synthesis method that directly results in electrically interconnected three-dimensional architectures is presented, where the carbon framework functions as current collector and lithium insertion material, eliminating the extra mass and expense of inactive materials in conventional designs. Fibrous carbon electrode materials are produced from solvent extracted lignin using scalable melt processing technology and thermal conversion methods. The resulting free-standing electrodes exhibit comparable electrochemical performance to commercial carbon-based anodes at a fraction of the materials and processing costs. Compositional and electrochemical characterization shows that carbonized lignin has a disordered nano-crystalline microstructure. The carbonized mats cycle reversibly in conventional aprotic organic electrolytes with Coulombic efficiencies over 99.9%. Moreover, lignin carbon fibers carbonized at 2000 °C can cycle reversibly in 1 M $LiPF_6$ in propylene carbonate.

1. Introduction

Significant market penetration of electric vehicles will require non-incremental improvements in battery pack specific energies and energy densities at lower costs. While there are many recent developments in battery technology, only materials that combine high performance with low-cost, processed using industrially scalable methods, are expected to be commercially relevant and have a noticeable impact on device implementation. State of the art lithium ion battery manufacturing already employs such low-cost materials, yet electrochemical energy storage is still too costly for mainstream automotive applications.[1] We address these issues by focusing on bulk synthesis of active battery materials directly into a three-dimensional architecture from renewable resources (lignin) using industrially scalable technologies. Moreover, we have developed synthesis methods that could lead to a redesign of battery manufacturing by eliminating the need for slurry coating processing.

Dr. W. E. Tenhaeff, Dr. O. Rios, Dr. K. More, Dr. M. A. McGuire
Materials Science & Technology Division
Oak Ridge National Laboratory
Oak Ridge, TN, 37831, USA
E-mail: wyatt.tenhaeff@rochester.edu

DOI: 10.1002/adfm.201301420

Graphite is the predominant anode material in commercial lithium ion cells[2] due to favorable electrochemical performance.[3,4] To improve upon the theoretical capacity of graphite, Li alloys, for example, Li-Si and Li-Sn, are being studied by research groups across the globe.[5] Large irreversible capacities associated with solid electrolyte interface (SEI) formation and large volume changes associated with lithium insertion and extraction are difficult challenges. While there is considerable effort in developing high-capacity, low-cost active materials, an equally fruitful approach to improving effective cell capacities while reducing cost is fabricating thicker electrodes and minimizing (or completely eliminating) the relative fraction of inactive components within the electrodes.[6,7] The copper current collector in the anode, in particular, adds significant mass and cost to the cell.[8] Anodes where copper is eliminated can have dramatic improvements in practical capacities and cost reductions.[9]

We have selected a naturally occurring carbon precursor and engineered its carbonized structure to yield an active material with an internally modulated mesostructure consisting of high-density, nanoscale crystalline (graphitic) domains surrounded by a continuous, low-density, highly disordered carbon matrix. The amorphous carbon enables facile, isotropic lithium transport[10] throughout the fiber structures, providing access to charge storage sites within the nanoscale graphitic domains while avoiding high specific surface areas associated with nanomaterials.

Lignin-based carbon fibers (LCFs) that are derived from fibrous hardwood sources were incorporated into monolithic, electrically interconnected, self-supporting electrodes for lithium ion battery anodes. A novel electrode synthesis method has been developed such that the LCFs function simultaneously as electrode active material and current collector by virtue of their mixed ionic/electronic conductivities. This dual functionality eliminates massive metallic current collectors and traditional polymeric binders required in conventional electrode designs; consequently, the entire mass is active toward lithium insertion. The renewable carbon precursor, lignin, is a branched polyaromatic macromolecule, resulting in a high char yield (over 40 wt%) after pyrolysis.[11] Lignin is the second most abundant naturally occurring biopolymer[12] and on average

comprises 18–35% of wood by weight.[13] It is a byproduct of the pulp and paper industry, produced at several millions of pounds per year.[14] Even though lignin is a waste product that is burned for heat and power,[15] post-production processing, such as extensive thermal and chemical treatments, can significantly increase the cost of the end product. Therefore, we have strictly focused on producing materials using low cost melt processing technology. The projected costs of LCFs are $3/lb for monolithic, electrically interconnected, self-supporting mats,[16] which is significantly less expensive than battery grade graphite powders ($12/lb for unprocessed battery grade graphite).[17]

2. Results and Discussion

The 3D interconnected LCF networks were prepared by a forced air driven melt processing technique termed melt blowing. A unique stabilization and carbonization protocol was developed specifically for energy storage applications. The conversion of the lignin fiber mat into a monolithic structure consists of two steps: oxidative stabilization and pyrolysis/carbonization. Lignin is a complex network of phenolic monolignol units bonded through an array of different inter-unit bonds.[14,18] Oxidative stabilization consists of heating the lignin fibers in air to break the weakest intermolecular bonds and subsequently oxidize and crosslink the molecules, which elevates the glass transition temperature (T_g).[19,20] Control of the T_g is required to maintain the fiber morphology during oxidative stabilization, while also allowing lignin to later tolerate pyrolysis temperatures.[21] To eliminate the binder and current collector from the anode construction, we have developed techniques to reproducibly fuse physically contacting fibers to form electrical interconnections and provide stable, free-standing, porous mats. Effectively controlling the extent of fiber-fiber fusion and mat density is accomplished by thermal management of exothermic reactions and transient rheological properties, resulting in a self-supporting, electrically connected monolithic mat. Fiber–fiber fusion is a major engineering challenge hindering the implementation of lignin carbon fibers in structural applications;[21] however, this controlled process is an integral part of producing a highly conductive 3D network of active materials, such as that shown in **Figure 1**. The digital image in Figure 1a shows carbonized mat samples that are produced at pilot scale production levels; and the electron images in Figure 1b,c reveal the fiber-fiber fusion. This technology is compatible with the production of fibrous electrodes that are near full density (>90 vol% LCF).

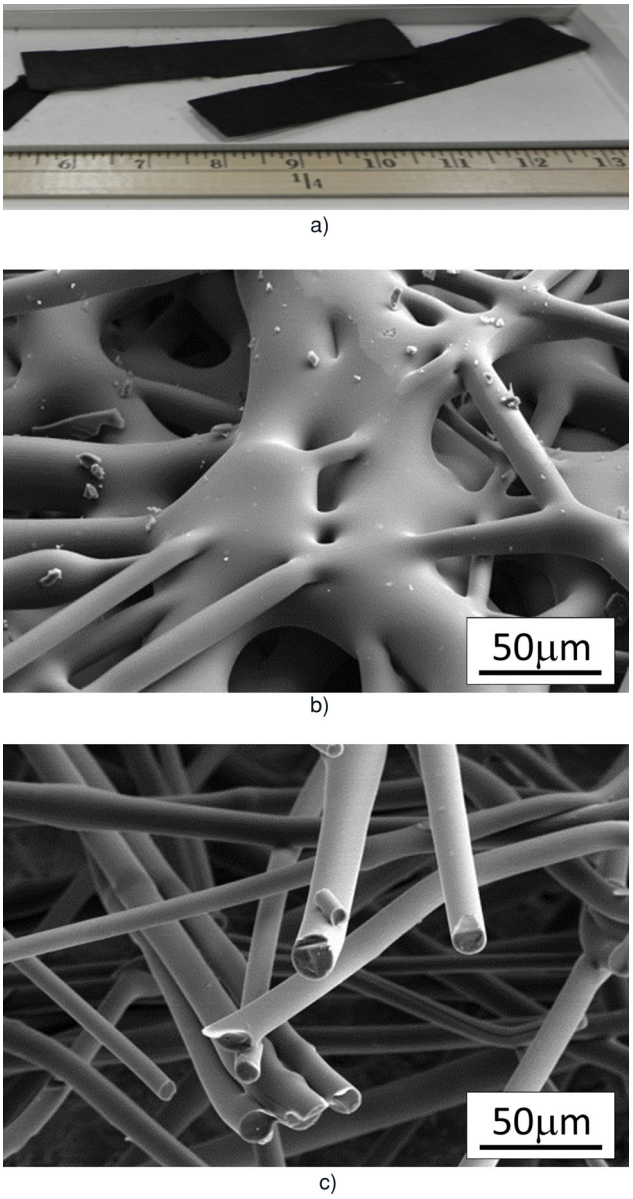

Figure 1. a) Digital image of typical LCF fused mats post-carbonization. b,c) Scanning electron images of varying levels of fiber–fiber fusion in LCFs mats, indicating that fusion and mat densities can be controlled through the fabrication process.

Conversion of the stabilized lignin into carbon fibers consists of pyrolyzing the lignin in an inert atmosphere to above 600 °C and releasing volatiles, resulting in a 50 to 60% reduction in mass along with a volumetric contraction of the fiber mat. On a molecular level, aromatic rings form graphite-like domains while linear branches are lost as hydrocarbons. In order to understand the role of microstructure on the electrochemical performance of LCFs as lithium ion anodes, a select series of LCF mats were synthesized using identical processing parameters with the exception of the carbonization temperature. Three carbonization temperatures were examined: 1000, 1500, and 2000 °C. High-resolution transmission electron microscopy (HR-TEM) imaging reveals that the conversion yields LCF microstructures with a perfectly disordered distribution of matrix crystallographic orientations and controllable degrees of matrix graphitization dependent on carbonization temperature, which is distinct from commercial carbon fiber microstructures.[22] A comparison of the fiber microstructures resulting from the three carbonization temperatures (**Figure 2**a–c) shows increased matrix graphitization with increasing temperature. Analysis of the (002), (100), and (110) obtained from selected area electron diffraction (SAED) indicates the development of increased long-range graphite order with no preferential orientation along the fiber direction. This observation was confirmed

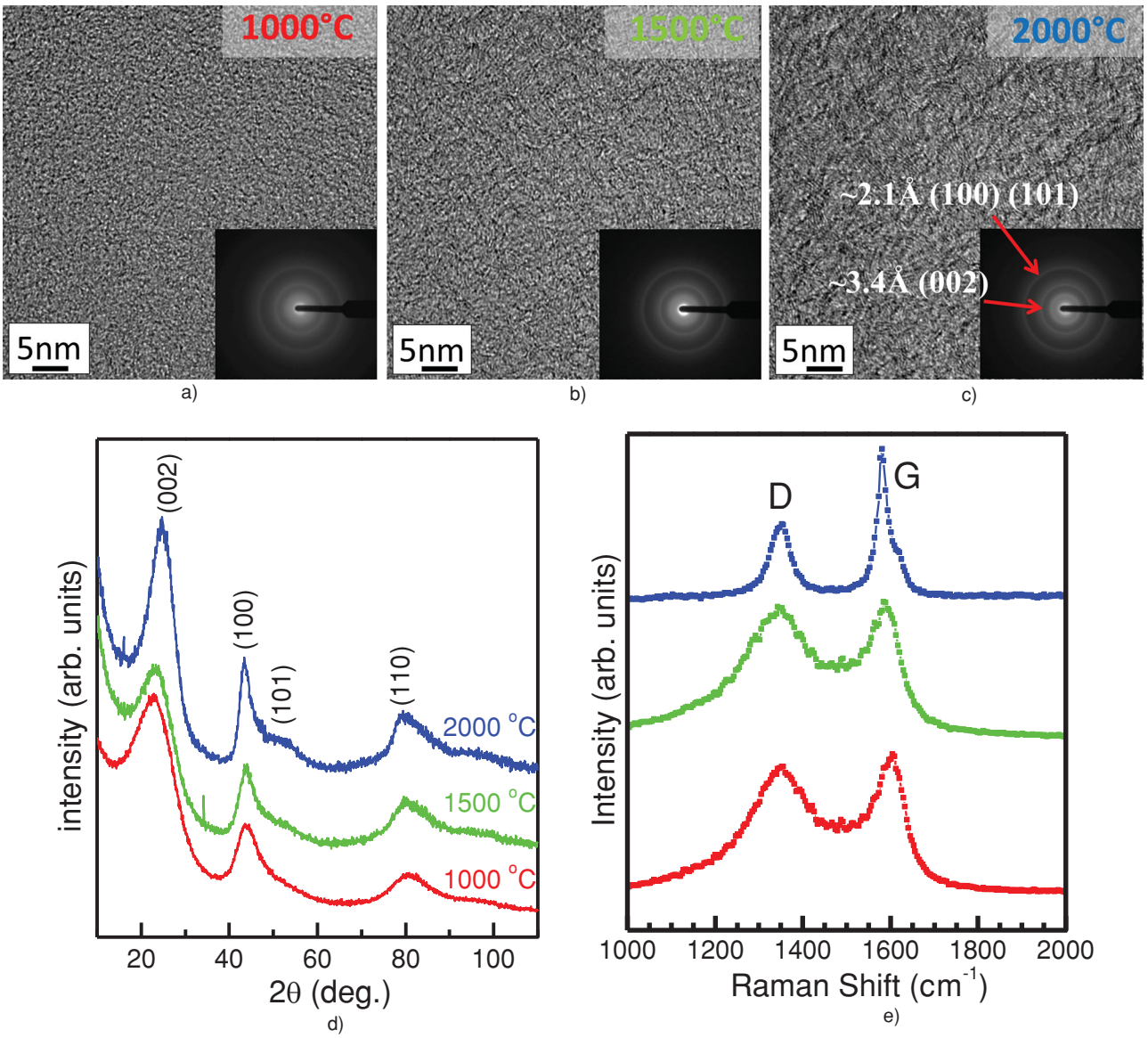

Figure 2. High resolution transition electron microscopy images at a) 1000, b) 1500, and c) 2000 °C. The inset images are selective area electron diffraction patterns on the same materials. d) X-ray diffraction patterns and e) Raman spectroscopy spectra for the LCFs carbonized at the same temperatures.

in X-ray diffraction (XRD) experiments on bulk powder samples, as shown in Figure 2d. Although the samples processed at higher temperatures exhibit somewhat sharper XRD peaks, all the observed reflections are broad for each of the three samples because the average graphite crystallite/domain size remains extremely small even though increased graphitization is observed with carbonization temperature. A lower bound of crystallite size can be obtained by assuming all of the observed broadening is due to the crystallite size effect. Analysis of the (002) reflection gives minimum average crystallite sizes of 0.9, 1.2, and 1.4 nm for carbonization temperatures of 1000, 1500, and 2000 °C, respectively. Similar analysis for the (100) reflection gives 1.8, 2.4, and 3.9 nm, respectively. Other sources of peak broadening are expected, in particular a high density of lattice defects or distortions between the graphitic basal planes. These effects can cause anisotropic and hkl-dependent broadening (as observed here for measurements using (100) and (002) reflections), which complicate analysis of the diffraction profiles. The appearance of the mixed (101) reflection in only the 2000 °C sample indicates the prevalence of translational stacking faults in these materials, and the shift of the (002) reflections to higher 2-theta with processing temperature indicates fluctuations in the *c*-axis interlayer spacing or distortion of the graphitic layers.[23] It is clear that long-range order along the *c*-axis of the graphitized domains increases with heat-treatment temperature. HR-TEM images reveal the evolution of nanoscale graphitic domains at 1500 °C, consistent with a slight decrease in the broadening of the XRD peaks observed between 1000 °C and 1500 °C. This suggests that the seemingly amorphous material in the as-processed LCF has comparable short-range order

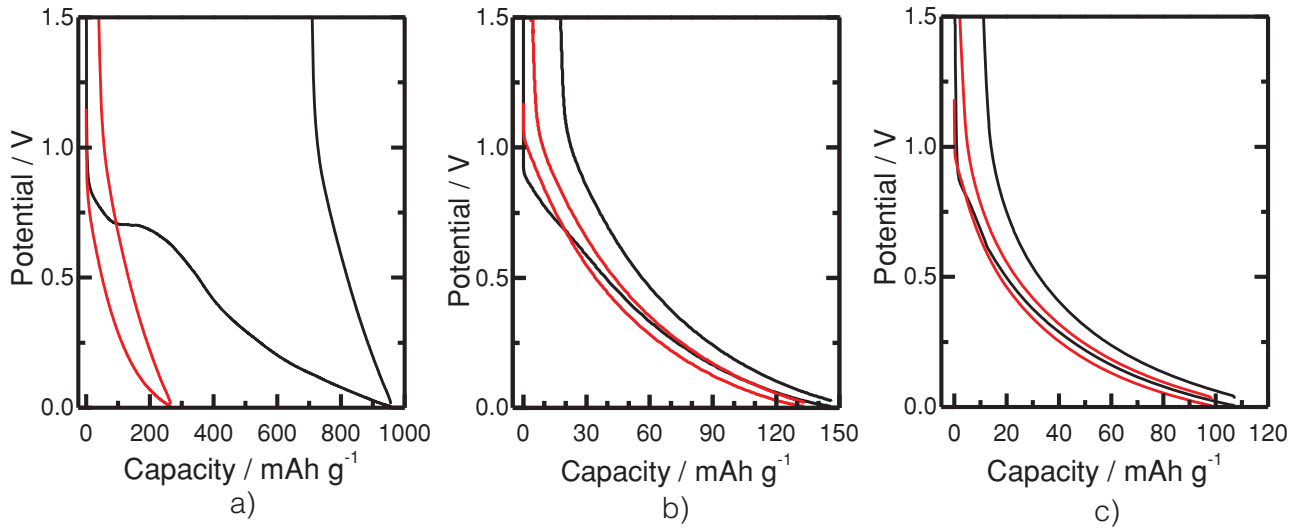

Figure 3. Voltage profile for first (black line) and second (red line) galvanostatic cycles of LCF mats carbonized at a) 1000, b) 1500, and c) 2000 °C. Rate is 7.5 mA g^{-1} and the electrolyte is 1.2 M $LiPF_6$ EC:DMC (3:7 v/v).

that evolves to exhibit a more graphitic structure within clearly identifiable domains in the 1500 °C sample, which is a result of enhanced ordering within nanoscale domains and an apparent increase in crystallinity.

Raman spectroscopy measurements were conducted to characterize the degree of graphitization as a function of carbonization temperature. Representative Raman spectra of the three LCFs are provided in Figure 2e. The D and G bands at ≈1360 and 1590 cm^{-1}, respectively, are clearly observed in all three spectra. The Raman spectra for 1000 and 1500 °C LCFs are similar, indicating a high degree of disorder, and closely resembling spectra from petroleum pitch-based carbon fibers[24] and carbon-black.[25,26] The reduced full-width half-maximum (FWHM) of the Raman bands in the LCFs carbonized at 2000 °C demonstrate the enhanced crystallinity (graphitization). This sample also shows the emergence of a shoulder on the high wavenumber side of the G band. The spectrum acquired for this sample is quite similar to that observed in nanocrystalline graphite.[24,27]

To quantify the effect of the carbonization temperatures on lithium storage capacity, the fused mats were incorporated into coin cells against Li metal counter electrodes. The voltage profiles of the first and second cycles provided in **Figure 3** do not reveal discernible staging, indicative of the disordered structure observed where Li storage sites within the LCFs are electronically and geometrically distinct.[28,29] This lack of staging is observed in several types of carbon fibers where long range crystalline order is absent.[30–33] Whereas the voltage profiles may resemble capacitive behavior, the contribution of capacitance to the measured specific capacities is quantified in the Supporting Information and is determined to be negligible. First cycle irreversible capacities, which are tabulated in **Table 1**, clearly diminish as the carbonization temperature increases. Irreversible capacities around 10 to 15% are consistent with

Table 1. Energy storage properties for the materials and electrode designs.

Material	Q_{irr} [%][a)]	Q_{360}/Q_{15}[b)]	$\overline{Q}$ [mAh g^{-1}][c)]	$\overline{CE}$[c)]	Loss [%][d)]
Slurry-coated					
1000 °C	19.1	0.96	349.8	99.60%	1.8
1500 °C	12.6	0.93	147.8	99.87%	1.4
2000 °C	12.1	0.96	126.1	99.89%	0.8
Fused mats					
1000 °C	73.2	0.75	193.0	99.85%	3.9
1500 °C	9.9	0.91	124.7	99.95%	1.9
2000 °C	9.5	0.92	95.8	99.95%	0.9

[a)] Defined as $[(Q_{D,1} - Q_{C,1})/Q_{D,1} \times 100]$%, where $Q_{D,1}$ and $Q_{C,1}$ is the lithiation and extraction capacity of the initial cycle, respectively. Note: plots of first cycle lithiation and extraction of the slurry-coated electrodes are provided in the Supporting Information; [b)] Q_{360} is the average lithium extraction capacity measured when the cells are cycled galvanostatically at 360 mA g^{-1}. Q_{15} is the average extraction capacity at 15 mA g^{-1}. Averages calculated using data in Figure 4c,d; [c)] Average specific charge capacity from cycle 1 to 70 in Figure 4e,f. Rate is 15 mA g^{-1}; [d)] Measure of loss in specific charge capacity over 70 cycles presented in Figure 4e,f. Defined as $[(Q_{C,1} - Q_{C,70})/Q_{C,1} \times 100]$%.

commercial graphite materials.[34] The dramatic difference in irreversible capacity between 1000 and 1500 °C is interesting given the similarity of their microstructures (see Figures 1,2). It is likely that 1000 °C is insufficient to completely eliminate organic functionalities within the fibers that irreversibly bind Li cations. Presumably, the quasi-plateaus at approximately 0.75 V in the first cycles are due to SEI formation.

The electrochemical performance of LCFs in two distinct electrode formats was compared. In one format, the LCFs were fused into monolithic mats and carbonized, and no further processing was performed. In this format, the carbon fibers function as both active charge storage media as well as the electronic current collector. The second format mimics traditional lithium ion battery electrode fabrications, where the LCFs were ground into fibrous powders and slurry coated as thin composite electrodes onto copper current collectors. Typical lengths of the ground fibers ranged from 50 to 150 μm, and the nominal coated electrode thickness was 60 μm. A scanning electron microscopy (SEM) image of the slurry-coated LCFs is provided in **Figure 4**a. The architecture of these electrodes is in stark contrast to the fused LCF mat electrodes, which appear in in Figure 4b.

The rate performance of the two electrode designs is presented in Figure 4c,d. Coin cells with Li metal counter electrodes were assembled and galvanostatically cycled between 5 mV and 1.5 V, with a potentiostatic hold at the bottom of the lithiation step (5 mV) until the current decayed below a threshold value of 5 μA. This cycling protocol measures the charge capacities at several extraction rates (discharge in a full cell). Cells were cycled at several rates incrementally. Capacity retention at high rates is clearly better in the slurry-coated electrodes. Table 1 also provides the capacity retentions at 360 mA g^{-1}, defined as Q_{360}/Q_{15}, where Q_n is the charge storage capacity measured at a rate of n mA g^{-1}. Capacity retentions are quite high for the slurry-coated electrodes with the fibers carbonized at 1500 °C, showing the most loss (7%) at 360 mA g^{-1}. This is consistent with the graphitic composite anodes optimized for transport.[35] While the capacity utilization at high rates is slightly reduced in the fused mats, the rate capabilities of these electrodes are still very good. For LCFs carbonized at 1500 and 2000 °C, over 90% of the capacity is accessed at 360 mA g^{-1}. The slight reduction in rate capabilities can be rationalized considering that the thicknesses of the LCF mats were nominally several hundreds of micrometers while the coated composite electrodes were only 60 μm thick. Consequently, concentration polarization will be more extensive in the LCF mats. It is important to note that these mats have not been optimized for charge transport considerations. Future efforts will emphasize controlling the fiber-fiber fusion for efficient electron transport while optimizing both the porosity and architecture of the mats for electrolyte wetting and volumetric densities.

The reversibility of lithium storage in LCFs in the two electrode designs were quantified and compared through extended galvanostatic cycling at 15 mA g^{-1}. Storage capacities over 70 cycles appear in Figure 4e,f and show that these materials reversibly store lithium. For clarity, Coulombic efficiencies (CEs) are not plotted within the figures; they can be found as a function of cycle number in the Supporting Information. The average Coulombic efficiency for the 70 cycles is recorded in Table 1 along with the average charge capacity. The average efficiencies being around 99.9% suggests that these materials are relevant for practical cells. The CEs for the two electrode designs are quite similar, with LCFs carbonized at 1500 and 2000 °C having the highest CEs. Moreover, the loss in extraction capacity over the 70 cycles is tabulated in Table 1. The LCFs carbonized at 2000 °C show the least amount of loss after 70 cycles (less than 1% for both electrode designs), and LCFs mats carbonized at 1000 °C lose the most. Considering the CEs and capacity loss results, it is clear that the LCF materials retain their good reversibility in the fused mat designs where the binder and copper current collector are eliminated.

The highest capacity was obtained in LCFs carbonized at 1000 °C. The average capacities of 1000 °C LCF in mats and slurry-coated electrodes were 193 and 350 mAh g^{-1}, respectively. For disordered carbons, the capacity is inversely related to the carbonization temperature.[36] The capacities of the 1500 and 2000 °C LCFs measured at 15 mA g^{-1} (provided in Table 1) are significantly lower than the 1000 °C LCFs. This is consistent with previous studies of disordered carbons, where closure of micro- and nano-porosity and/or the turbostratic misalignment between the *c*-axis layers within the graphitic domains results in lower reversible capacities.[36,37] Comparing the average capacities of the two electrode designs reveals that higher specific capacities are obtained for LCFs coated onto copper current collectors. While a moderate difference between the coated and mat electrode designs is observed at 1500 and 2000 °C, the capacity of the 1000 °C LCFs is much higher in the slurry-coated electrodes. Multiple samples show consistent results. The mats carbonized at 1000 °C were noticeably brittle, and it is possible that sections of the mat broke during coin cell assembly, leading to electrically isolated regions within the electrode that did not participate electrochemically. This would result in the lower capacity measured in the 1000 °C mats.

The utility of the fused mat electrode designs becomes apparent by normalizing the capacities to the entire electrode masses. In the slurry-coated electrode, copper current collector, PVDF binder, and conductive additive contribute mass and volume but not capacity. In a typical commercial high energy 100 Ah lithium ion cell, the overall specific capacity of the cell is 129 mAh g^{-1}.[8] In the hypothetical case, where the theoretical capacity of graphite is utilized in these 100 Ah cells (i.e., the cells are not oversized), the overall specific capacity is 267 mAh g^{-1}. These estimates clearly highlight the importance of minimizing inactive components. The overall capacity of the 1000 and 1500 °C LCF mats compare well with conventional slurry-coated graphite anodes while circumventing the inherent inefficiencies of slurry-coated electrode technology.

The choice of electrolyte is a further consideration for carbon charge storage materials. Electrolytes containing propylene carbonate (PC) are preferred over ethylene carbonate (EC) for low temperature operation, an important metric for automotive applications, because the melting point of PC is –48.8 °C compared to 36.4 °C for ethylene carbonate.[38] Graphite exfoliates in PC due to solvent co-intercalation. As graphite exfoliates, it exposes new surface area, resulting in continued SEI formation and indefinite irreversible capacity.[39,40] This behavior of graphite precludes the use of PC-based electrolytes. LCFs in

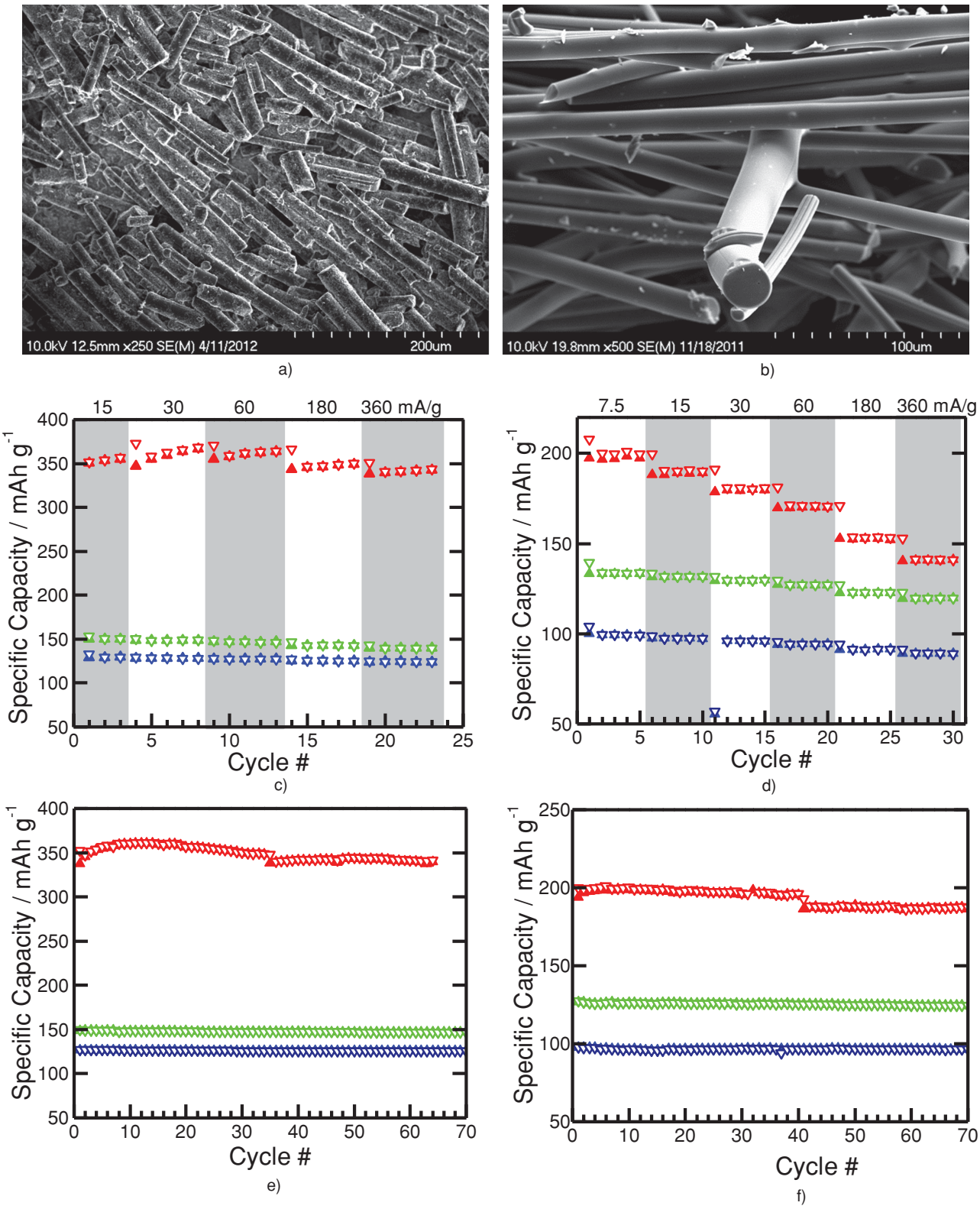

Figure 4. Scanning electron images of LCFs a) ground for particle size reduction and coated onto copper current collectors by slurry coating and b) fused into electrically interconnected mats. Charge storage capacity of LCFs carbonized at 1000 (red), 1500 (green), and 2000 °C (blue) as a function of current in c) slurry-coated electrodes and d) fused mats. Charge capacities as a function of cycling and carbonization temperatures in e) slurry-coated electrode and f) fused mats. For all data, the counter-electrode is Li metal and the electrolyte is 1.2 M $LiPF_6$ in EC:DMC (3:7 v/v).

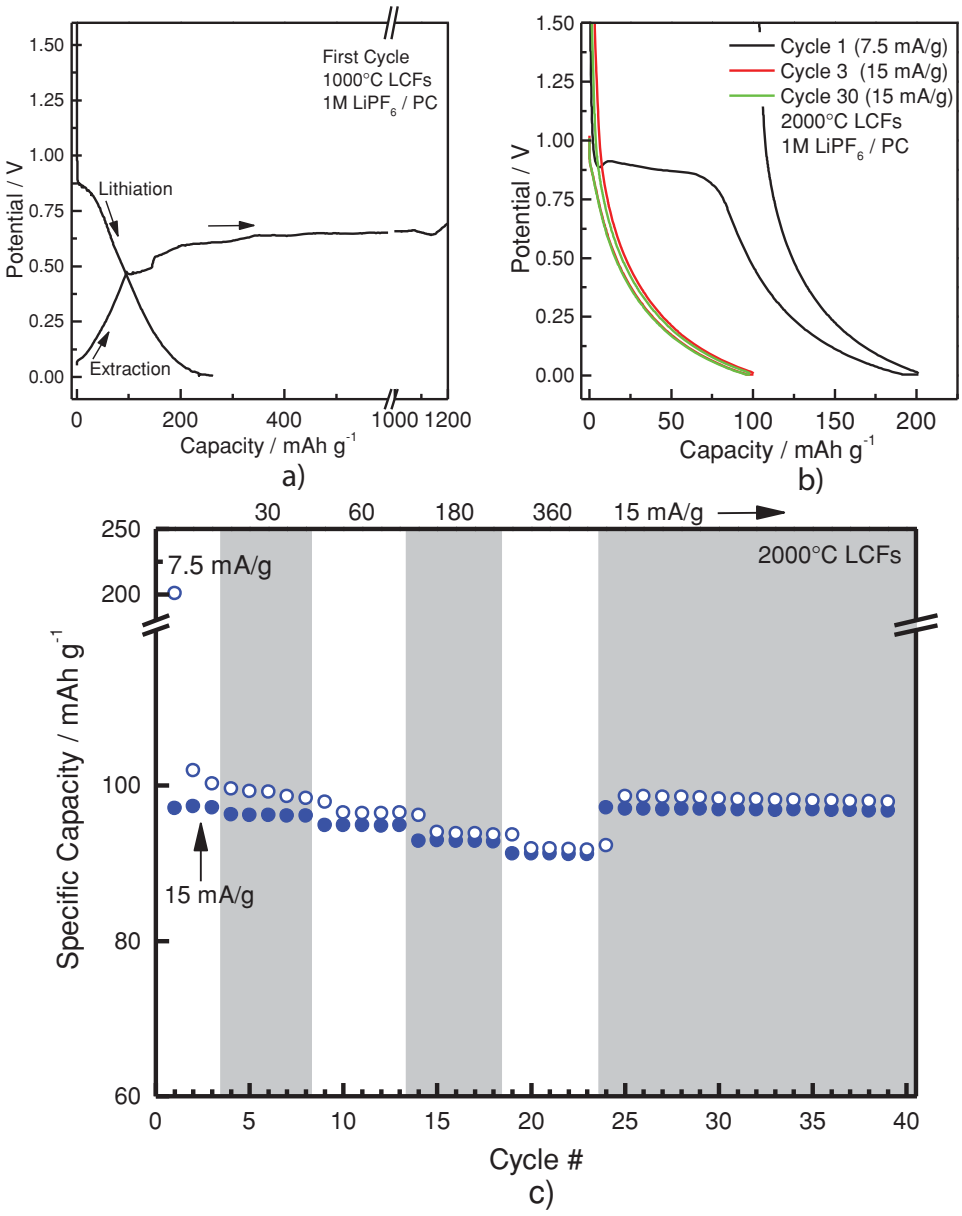

Figure 5. Galvanostatic voltage profiles for the lithiation and extraction of Li in LCFs carbonized at a) 1000 °C and b) 2000 °C in 1 M $LiPF_6$ in PC. CE: Li metal. c) Capacity of the 2000 °C LCFs as a function of cycling against Li metal with capacity retention measured at several rates as indicated on the top of the plot.

fused mat electrodes were cycled in PC to assess the stability of the unique LCF microstructure and morphology. Voltage profiles for lithiation and extraction of LCFs carbonized at 1000 and 2000 °C are shown in **Figures 5**a,b. It is intriguing that little SEI formation is observed during the lithiation of 1000 °C LCFs. The capacity obtained in this first cycle is consistent with the reversible capacity in ethylene carbonate (EC)/dimethyl carbonate (DMC) mixtures (see Figure 4D). The 1000 °C materials, however, cannot be galvanostatically charged to the cut-off voltage of 1.5 V; rather, there is an indefinite plateau at 0.6 V, the origin of which is not understood at this time. The measured capacity clearly cannot be solely attributed to lithium extraction. For this reason, the charging profile was not plotted as the reverse of lithiation (Figure 5a) as is done in the other figures.

The scenario is completely different for LCFs carbonized at 2000 °C. In the first lithiation step, an appreciable SEI develops, as indicated by the voltage plateau. The plateau does not extend indefinitely, as observed for graphite in PC,[40] and the material successfully lithiates to 5 mV. The first extraction capacity is consistent with the capacities obtained in EC/DMC electrolytes. After the first cycle, the LCFs cycle reversibly. High Coulombic efficiencies are achieved during the rate performance steps and extended cycling at 15 mA g^{-1}, and the capacity is stable to at least 40 cycles. The capacities are slightly lower in PC, presumably due to the resistance of the SEI layer. The behavior of LCFs

in PC is intriguing as one might expect the LCFs carbonized at 2000 °C to fare worse in PC given their enhanced graphitic nature.[41,42] LCFs carbonized at 1000 °C have the greatest extent of disorder and should inhibit PC co-intercalation. This behavior needs to be investigated further, but it effectively illustrates the importance of the distinct LCF microstructure and morphology in defining unique electrochemical performance.

3. Conclusions

The electrochemical performance of LCFs with engineered disordered microstructures and fibrous morphologies have been presented. We have demonstrated specific charge capacities in LCF materials produced from inexpensive, abundant, and renewable resources, using a cost-effective and industrially scalable technique that rival current state of the art electrode designs. When synthesized as monolithic fused mats to function as both the active material and current collector, these LCFs have specific charge capacities comparable to conventional graphitic anodes in lithium-ion batteries when normalized by the total mass of the anode assembly. LCFs carbonized at 1000 °C have the highest specific charge capacities. Carbonization of LCFs at high temperatures resulted in greater graphitization and lower specific charge capacities, but significant improvements in first cycle efficiencies were observed. The unique electrochemical behavior of LCFs was further highlighted through the characterization of cycling in PC electrolyte. Stable cycling of LCFs carbonized at 2000 °C, which had the greatest graphitic content, was demonstrated in solutions of $LiPF_6$ in PC for over 40 cycles. Irreversible lithium insertion and extraction was observed in the more disordered LCFs carbonized at 1000 °C with the smallest nanoscale graphitic domains.

4. Experimental Section

Solvent extracted hardwood using the Alcel extraction process was prepared by melt blowing fibers 8–15 μm fibers onto a polyethylene support structure forming a lignin fiber mat with a nominal thickness of 1.2 cm in batches of at least 25 lbs demonstrating scalability of this technology. The lignin fiber mat was oxidatively stabilized in a convection furnace by heating the materials to 250 °C at sufficiently fast rates to fuse the fiber mat without fully melting the materials (typically between 0.01 °C and 1 °C min^{-1}). Pyrolysis and carbonization were performed by heating the materials in flowing Argon gas up to the annealing temperature (1000, 1500, or 2000 °C) at a nominal rate of 3 °C min^{-1} and cooling at a rate of 3 °C min^{-1}. The flowing gas was used to remove the volatile compounds that are produced during pyrolysis. Approximately 60% of the green fiber mass is lost during pyrolysis at 600 °C, and the carbon yield remains constant above 700 °C.

Scanning electron microscopy (SEM) was performed using a JEOL 6500F SEM with a 10 keV accelerating voltage in secondary electron imaging mode. Individual LCF cross-sections were prepared for HR-TEM by using the focused ion beam (FIB) lift-out method (NB5000 FIB-SEM, Hitachi). A Ga^+ ion beam (40 kV) was used to section and thin the single fibers to transparency. A final 2 kV "surface polish" was used to remove damage from the FIB specimen surface. High-resolution TEM imaging of the LCF specimens was performed in a Hitachi HF3300 operated at 300 keV. Raman spectroscopy of the carbonized LFCs prior to electrochemical characterization was conducted using an Alpha 300 confocal micro-Raman instrument (WITec Inc.). A solid-state 532 nm excitation laser with a 20× objective and 600 grooves per millimeter grating was used for the Raman microscopy. Samples for powder X-ray diffraction were prepared by gently hand-grinding the fibers in a mortar and pestle. Data was collected with a PANalytical X'Pert Pro MPD diffractometer using Cu $K\alpha_1$ radiation.

Two LCF electrode formats were characterized. For the first electrode design, 9.5 mm discs were punched from the fused lignin mats. Thicknesses of the mats varied from sample to sample, but were typically between 200 to 400 μm thick. The second design mimicked conventional lithium ion battery electrodes. The fused LCF mats were ground into a powder; the fibrous morphology was retained, but the aspect ratios were reduced and fiber-fiber interconnections broken. The LCF powders were mixed with poly(vinylidene diflouride) (PVDF) binder purchased from Sigma-Aldrich and conductive carbon additives (Super C65, Timcal) in the mass ratio 83:15:2. The mixture was added to anhydrous N-methyl pyrrolidinone (99.5% purity, Sigma-Aldrich) to make a viscous slurry. The slurry was coated onto copper foil as a 100 μm thick wet coating using a doctor blade. The slurry was dried and the total electrode assembly was pressed to a thickness of 75 μm. Electrodes with 9.5 mm diameters were punched from the coated copper foil. For both formats, the nominal loading of LCFs in the electrodes was 5 mg cm^{-2}. The punched electrodes were transferred to an Ar-filled glovebox with a moisture level less than 1 ppm and dried to remove residual adsorbed moisture.

After drying, the electrodes were assembled into coin cells. Celgard 2325 and Li metal were used as separator and counter electrode, respectively. Lithium ion battery grade electrolyte, 1.2 M $LiPF_6$ in ethylene carbonate/dimethyl carbonate (3:7 v/v), was purchased from Novolyte. For a few experiments with LCF mats, a 1 M $LiPF_6$ solution in anhydrous propylene carbonate (PC) (99.7% purity, Sigma-Aldrich) was used as the electrolyte. The $LiPF_6$ (99.99% purity, Sigma-Aldrich) was dried in vacuum at 150 °C under vacuum for 24 h prior to mixing into the PC. For this electrolyte, a glass fiber membrane (Whatman) was employed as the separator.

The cells were cycled galvanostatically from 1.5 to 0.005 V on a Maccor 4000 battery cycler. For the rate performance characterization, a potentiostatic step at 5 mV was implemented during lithiation, and 5 μA was used as the cut-off threshold. Initially, low currents were employed, and then incrementally increased to a maximum of 360 mA g^{-1}. The rates are indicated in the figures. Extended cycling was also performed over 70 cycles at a rate of 15 mA g^{-1}. The cycling protocol was slightly altered; the potentiostatic step was at 1.5 V to ensure complete lithium extraction.

Supporting Information

Supporting Information is available from the Wiley Online Library or from the author.

Acknowledgements

W.E.T. and O.R. contributed equally to this work. Research sponsored by the Laboratory Directed Research and Development Program of Oak Ridge National Laboratory, managed by UT-Battelle, LLC, for the U. S. Department of Energy. Research was also supported by ORNL's Shared Research Equipment (ShaRE) User Program, which is sponsored by the Office of Basic Energy Sciences, U.S. Department of Energy. X-ray diffraction studies were supported by the U.S. Department of Energy, Basic Energy Sciences, Materials Sciences and Engineering Division. The authors thank Dr. Jagjit Nanda for the use of his Raman microscope, which is supported by the Assistant Secretary for Energy Efficiency and Renewable Energy, Office of Vehicle Technologies of the U.S. Department of Energy, and Dr. Surendra Martha for his technical insights regarding electrochemical characterization of carbon fiber materials.

Received: April 25, 2013
Revised: June 13, 2013
Published online: August 9, 2013

[1] J.-M. Tarascon, *Philos. Trans. R. Soc. A* **2010**, *368*, 3227.
[2] K. Xu, *Chem. Rev.* **2004**, *104*, 4303.
[3] K. Kinoshita, K. Zaghib, *J. Power Sources* **2002**, *110*, 416.
[4] M. Winter, J. O. Besenhard, M. E. Spahr, P. Novak, *Adv. Mater.* **1998**, *10*, 725.
[5] W. J. Zhang, *J. Power Sources* **2011**, *196*, 13.
[6] W. Lai, C. K. Erdonmez, T. F. Marinis, C. K. Bjune, N. J. Dudney, F. Xu, R. Wartena, Y. M. Chiang, *Adv. Mater.* **2010**, *22*, E139.
[7] X. Qin, X. H. Wang, J. Xie, L. Wen, *J. Mater. Chem.* **2011**, *21*, 12444.
[8] *Costs of Lithium-Ion Batteries for Vehicles*, U.S. Department of Energy, 2000.
[9] http://www.transportation.anl.gov/batteries/assessment.html (accessed: August 2012)
[10] M. Park, X. C. Zhang, M. D. Chung, G. B. Less, A. M. Sastry, *J. Power Sources* **2010**, *195*, 7904.
[11] R. K. Sharma, J. B. Wooten, V. L. Baliga, X. H. Lin, W. G. Chan, M. R. Hajaligol, *Fuel* **2004**, *83*, 1469.
[12] G. Milczarek, O. Inganas, *Science* **2012**, *335*, 1468.
[13] D. Dimmel, in *Lignin and Lignans: Advances in Chemistry*, (Eds: C. Heitner, D. Dimmel, J. A. Schmidt), CRC Press, Boca Raton **2010**.
[14] T. Saito, R. H. Brown, M. A. Hunt, D. L. Pickel, J. M. Pickel, J. M. Messman, F. S. Baker, M. Keller, A. K. Naskar, *Green Chem.* **2012**.
[15] A. J. Ragauskas, C. K. Williams, B. H. Davison, G. Britovsek, J. Cairney, C. A. Eckert, W. J. Frederick, J. P. Hallett, D. J. Leak, C. L. Liotta, J. R. Mielenz, R. Murphy, R. Templer, T. Tschaplinski, *Science* **2006**, *311*, 484.
[16] Cost Modeling of Alternative Carbon Fiber Manufacturing Technologies – Baseline Model Demonstration Oak Ridge National Laboratory report to Department of Energy Vehicle Technologies Program, 2012.
[17] C. Daniel, *JOM* **2008**, *60*, 43.
[18] H. Nimz, *Angew. Chem. Int. Ed.* **1974**, *13*, 313.
[19] J. L. Braun, K. M. Holtman, J. F. Kadla, *Carbon* **2005**, *43*, 385.
[20] C. Crestini, M. Crucianelli, M. Orlandi, R. Saladino, *Catal. Today* **2010**, *156*, 8.
[21] D. A. Baker, N. C. Gallego, F. S. Baker, *J. Appl. Polym. Sci.* **2012**, *124*, 227.
[22] R. Perret, W. Ruland, *J. Appl. Crystallogr.* **1970**, *3*, 525.
[23] Z. Q. Li, C. J. Lu, Z. P. Xia, Y. Zhou, Z. Luo, *Carbon* **2007**, *45*, 1686.
[24] A. Cuesta, P. Dhamelincourt, J. Laureyns, A. Martinezalonso, J. M. D. Tascon, *Carbon* **1994**, *32*, 1523.
[25] A. Sadezky, H. Muckenhuber, H. Grothe, R. Niessner, U. Poschl, *Carbon* **2005**, *43*, 1731.
[26] T. Jawhari, A. Roid, J. Casado, *Carbon* **1995**, *33*, 1561.
[27] G. Irmer, A. Dorner-Reisel, *Adv. Eng. Mater.* **2005**, *7*, 694.
[28] P. Novak, D. Goers, M. E. Spahr, in *Carbons for Electrochemical Energy Storage and Conversion Systems*, (Eds: F. Beguin, E. Frackowiak), CRC Press, Boca Raton **2009**, 263.
[29] M. Winter, J. O. Besenhard, in *Hanbook of Battery Materials*, (Eds: C. Daniel, J. O. Besenhard), Wiley VCH, Weinheim **2011**.
[30] V. Subramanian, H. W. Zhu, B. Q. Wei, *J. Phys. Chem. B* **2006**, *110*, 7178.
[31] J. F. Snyder, E. L. Wong, C. W. Hubbard, *J. Electrochem. Soc.* **2009**, *156*, A215.
[32] R. Kanno, Y. Kawamoto, Y. Takeda, S. Ohashi, N. Imanishi, O. Yamamoto, *J. Electrochem. Soc.* **1992**, *139*, 3397.
[33] N. Imanishi, H. Kashiwagi, T. Ichikawa, Y. Takeda, O. Yamamoto, M. Inagaki, *J. Electrochem. Soc.* **1993**, *140*, 315.
[34] F. Ding, W. Xu, D. W. Choi, W. Wang, X. L. Li, M. H. Engelhard, X. L. Chen, Z. G. Yang, J. G. Zhang, *J. Mater. Chem.* **2012**, *22*, 12745.
[35] H. Buqa, D. Goers, M. Holzapfel, M. E. Spahr, P. Novak, *J. Electrochem. Soc.* **2005**, *152*, A474.
[36] J. R. Dahn, T. Zheng, Y. H. Liu, J. S. Xue, *Science* **1995**, *270*, 590.
[37] E. Buiel, J. R. Dahn, *Electrochim. Acta* **1999**, *45*, 121.
[38] Y. P. Wu, C. R. Wan, C. Y. Jiang, S. B. Fang, Y. Y. Jiang, *Carbon* **1999**, *37*, 1901.
[39] M. Arakawa, J. I. Yamaki, *J. Electroanal. Chem.* **1987**, *219*, 273.
[40] S. K. Jeong, M. Inaba, R. Mogi, Y. Iriyama, T. Abe, Z. Ogumi, *Langmuir* **2001**, *17*, 8281.
[41] M. Herstedt, A. M. Andersson, H. Rensmo, H. Siegbahn, K. Edstrom, *Electrochim. Acta* **2004**, *49*, 4939.
[42] D. Aurbach, H. Teller, E. Levi, *J. Electrochem. Soc.* **2002**, *149*, A1255.